Sensors **2004**, *5*, 58-70

sensors

ISSN 1424-8220
© 2004 by MDPI
http://www.mdpi.net/sensors

p-n Junction Photocurrent Modelling Evaluation under Optical and Electrical Excitation

Constantine T. Dervos [1]*, **Panayotis D. Skafidas** [1], **John A. Mergos** [1] **and Panayota Vassiliou** [2]

National Technical University of Athens 9, Iroon Polytechniou Str, Zografou 157 73, Athens, Greece

[1] Department of Electrical and Computer Engineering.

[2] Department of Chemical Engineering

* Author to whom correspondence should be addressed. E-mail: cdervos@central.ntua.gr

Received: 10 May 2004 / Accepted: 14 June 2004 / Published: 20 July 2004

Abstract: Based upon the quasi-equilibrium approximation, the validity of p-n junction modelling, has been experimentally investigated under synchronous electrical and optical excitation of silicon photo-diodes. The devices had areas of 8.2 mm^2 and reverse bias saturation currents of the order of 10^{-10} A. Their current-voltage (I-V) response was exploited experimentally both in the dark and under various illumination levels. The quoted values for the saturation current, the ideality factor, the series resistance and the reverse-bias photocurrent are investigated for the simulation of the I-V curves via the quasi-equilibrium model. In addition, the measured I-V data have been further analysed to estimate the produced photocurrent as a function of the applied bias (forward or reverse) under given illumination levels. Comparisons between the simulated curves and the experimental data allowed a detailed photocurrent modelling validation. The proposed approach could be useful towards studying other parameters of optically activated p-n junctions such as: the bias dependence of the minority carrier diffusion lengths and/or the generated rates of electron-hole pairs (EHP).

Keywords: Semiconductor applications, photovoltaics, p-n junction modelling, photocurrent.

Introduction

The modelling of photovoltaics (system or devices) is frequently employed by researchers in the field towards further analysis and understanding interactions between light and matter [1-4]. The determination of the current-voltage equation for the illuminated p-n junctions has been based upon the "quasi-equilibrium" approximation. That means, the quasi-Fermi levels for holes and electrons, Φp and Φ_n, respectively, remain flat all the way through the depletion layer width [5]. The application of an external bias, V_{fwd} or V_{rev}, splits the quasi-Fermi levels (depending on polarity) by the amount $q.V_{fwd}$, or $q.V_{rev}$. The component side sustaining the negative polarity is shifted towards higher electron potential energies (P.E.) compared to the component side sustaining the positive polarities, as shown in Fig. 1 [6].

When the p-n junction is illuminated by photons having an energy $h.\nu \geq E_g$, an added generation rate gopt (EHP/cm3-sec) participates in the overall current flow. The generated minority carriers, either within the depletion layer width, or within the minority carrier diffusion lengths at either side of the junction, are separated by the build-in electrostatic field, as shown in Fig. 2.

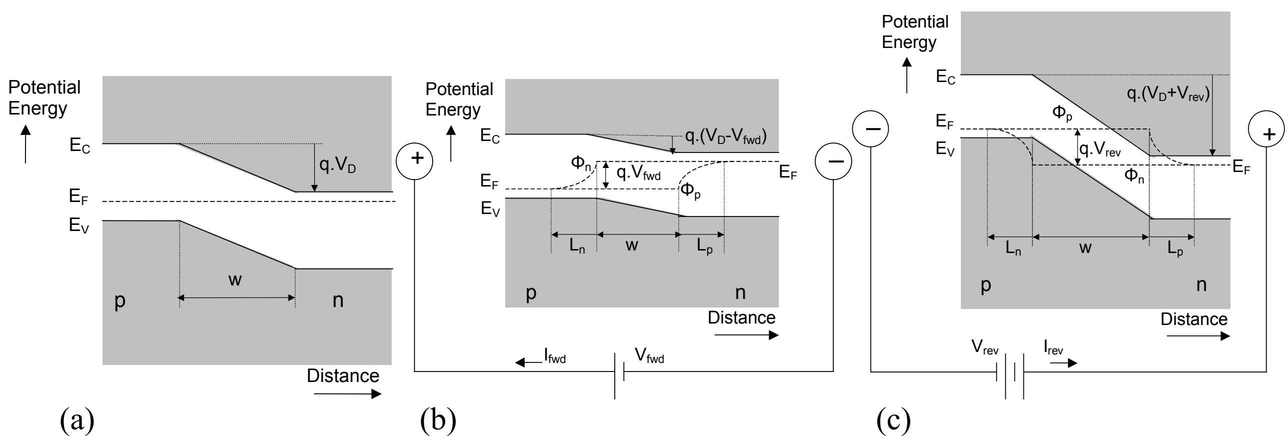

Figure 1. Quasi-equilibrium approximation and the potential energy band diagram as a function of distance for the case of a p-n junction **(a)** without externally applied bias, **(b)** under forward bias V_{fwd}, and **(c)** under reverse bias V_{rev}. Symbol list: E_c is the bottom of the conduction band, E_v is the top of the valence band, Φ_n and Φ_p are the quasi-Fermi levels for electrons and holes, E_F is the Fermi level at thermodynamic equilibrium, L_n and L_p are the minority carrier diffusion lengths for electrons and holes, V_D is the diffusion potential, w is the depletion layer width, q is the electronic charge and V_{TOTAL} is the junction total potential due to the applied bias (after [5]).

The absorption of photons leads to the formation of excess electrons in the n-side and excess holes in the p-side of the device, generating a voltage drop Voc across the p-n junction. The optically induced voltage splits the quasi-Fermi levels Φn and Φp by the amount q.Voc.

It can be shown that for an open circuit ideal junction (I=0), the developing voltage due to the photovoltaic effect (V=Voc) will be given by [7,8]:

$$V_{oc} = \frac{k.T}{q}.\ln\left(\frac{L_p + L_n}{(L_p/\tau_p)p_n + (L_n/\tau_n).n_p}.g_{opt} + 1\right) \tag{1}$$

where L_p, L_n are the minority carrier diffusion lengths (shown in Fig. 2), τ_p, τ_n are the minority carrier lifetimes, and p_n, n_p are the minority carrier densities.

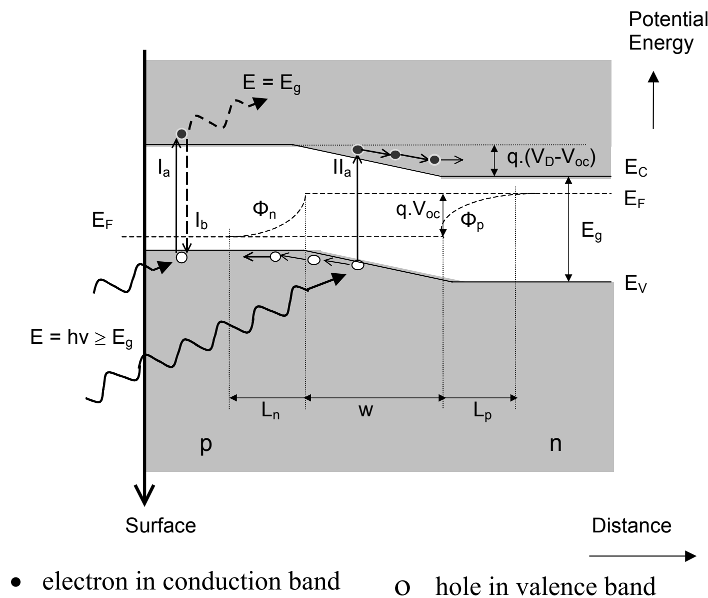

• electron in conduction band o hole in valence band

Figure 2. The produced electron-hole pairs within the depletion layer width or within the minority carrier diffusion lengths at either side of the junction (process II_a) separated by the build-in electrostatic potential, as shown by the small arrows for electrons in the conduction band and holes in the valence band. On the other hand, the electron-hole pairs induced by absorbed photons outside the aforesaid region (process I_a) will not be separated by the electrostatic field and once, the carriers lifetime has elapsed, they will recombine spontaneously, emitting photons having a total energy equal to the energy gap, E_g (process I_b).

According to the superposition principle, in the generalized case of a simultaneous electrical and optical excitation, the quasi-Fermi levels will split by the amount $q.V_{TOTAL}$, where $V_{TOTAL} = (V_{oc}+V_{fwd})$ or, $V_{TOTAL} = (V_{oc}-V_{rev})$ for the forward and reverse bias, respectively. Based on the "quasi-equilibrium" approximation, it can be shown that the analytical expressions for the current-voltage characteristics in any illuminated p-n junction will be given by [7,8]:

$$I_{fwd} = I_s \cdot \left(e^{\frac{qV_{fwd}}{kT}} - 1 \right) - qA(L_n + L_p).g_{opt} \tag{2}$$

$$I_{rev} = I_s + qA(L_n + L_p).g_{opt} \tag{3}$$

where I_{fwd} and I_{rev} are the forward and reverse net-flowing currents respectively, I_s is the saturation current in the dark, V_{fwd} is the applied forward bias, k is the Boltzmann constant, T is the junction absolute temperature, q is the electronic charge, A is the area of the device, L_p and L_n are the minority carrier diffusion lengths for holes and electrons, respectively, and g_{opt} is the optically induced generation rate for holes in the valence band and electrons in the conduction band.
The saturation current is given by [7,8]:

$$I_s = qA\left\{n_{po}\frac{D_n}{L_n} + p_{no}\frac{D_p}{L_p}\right\} = qAn_i^2\left\{\frac{D_n}{N_A L_n} + \frac{D_p}{N_D L_p}\right\} \quad (4)$$

where D_p and D_n are the minority carrier diffusion constants for holes and electrons, N_A and N_D are the ionized impurity concentrations for acceptors and donors, and n_{po} and p_{no} are the minority carrier concentrations under thermal equilibrium.

According to the Eqn. (2), in the forward biased p-n junction, the illumination produces a photocurrent component that reduces the net current flow (i.e., under given forward bias settings, less current flows in an illuminated device compared to the corresponding current that flows in the dark). In the reverse biased p-n junction, the produced photocurrent adds to the net current flow (i.e., the current that flows in a reverse biased illuminated device, equals the dark saturation current increased by the amount of the produced photocurrent).

The effect of recombination centers in a non-ideal p-n junction

Discrepancies from the theoretically predicted I-V characteristics of the quasi-equilibrium p-n junction model may rise by the presence of recombination centers in the junction area. Such centers may be distributed either in the bulk or over the surface, and they are physically related to the presence of deep electronic states in the band-gap of the materials, their energy distribution (E_T) and their exact corresponding concentration profile (N_T) [9]. Recombination states have been attributed either to crystal defects, or to the presence of contaminants. Recombination effects developing either within the depletion layer width (w) or within the minority carrier diffusion lengths at each side of the p-n junction (L_n, L_p) contribute significantly to the overall current flow across the barrier and affect forward and reverse I-V characteristics.

Forward bias

In a forward biased p-n junction, the recombination current density, J_{rec}, has been described by the Schockley-Read low level injection theory [10], which after certain simplifying assumptions, provides for this additional current component an equation of the following form [11]:

$$\left|J_{rec}\right| = q\cdot\int_{x=0}^{w} R.dx = \frac{q.w.n_i}{2.\tau_o}.e^{q.V_{fwd}/2.k.T} \quad (5)$$

where R is the recombination rate within the depletion layer width (w), n_i is the intrinsic carrier concentration, and $1/\tau_o$ is the recombination life-time. According to Eqn. (5), the recombination current dominates for forward applied voltages less than k.T/q. In this voltage range $0 \leq V_{fwd} \leq$ (k.T/q $\cong$ 25 mV at room temperature), the recombination current can be singularly identified in a log-linear I-V plot, since the resulting curve exhibits slopes of 2k.T/q instead of k.T/q as predicted for the ideal p-n junction (Eqn. 2).

Reverse bias

In the reverse bias, the presence of recombination centers affects the overall current-voltage characteristics by the generation of additional electron-hole pairs within the depletion layer width. Their generation rate, U, has been studied in the theory proposed by Shockley and Read, which after certain simplifying assumptions, leads to the following equation [11]:

$$U = \frac{\sigma.\upsilon_{th}.N_T.n_i}{2.\cosh\left(\frac{E_i - E_T}{k.T}\right)} \tag{6}$$

where σ is the trap cross-section, υ_{th} the defect thermal velocity, N_T is the concentration of the deep electronic states in the band gap distributed at energy levels E_T, and E_i is the intrinsic Fermi level.

The resulting current density due to the aforesaid current generation mechanism in a reverse biased p-n junction (in the depletion layer width), is given by the following equation [11]:

$$J_{gen} = q.\int_{x=0}^{w} U.dx = q.U.w \tag{7}$$

where an uniform generation rate throughout the depletion layer width has been assumed, i.e. a homogeneous defect concentration.

According to Eqn. (6) the generation rate of carriers (U) in the depletion layer width (w) will become maximum when $E_T \rightarrow E_i = E_g/2$. In addition, since the intrinsic concentration is a function of the energy gap of the material ($n_i \propto e^{-Eg/kT}$), it may be shown that semiconductors with small energy gaps will exhibit high generation rates, U [12]. The existing theory assumes that U is stable and uniform throughout the p-n junction region and that it remains independent of the applied bias. The proposed experimental approach might be useful towards the investigation of such statements.

Experimental and Discussion

In this work, the response of current-voltage characteristic of p-n junction photo-diodes has been experimentally studied under the combined action of illumination and externally applied dc bias. The employed devices consist of Si p-n junction photodiodes having areas of 8.2 mm^2 and reverse bias saturation currents in the dark as low as 10^{-10} A. Their I-V characteristics were measured under both

forward and reverse polarity, for voltage varying between V_{rev}= -1 V and V_{fwd} = +0.6 V, with 0.01 V increment. Measurements were accomplished by employing a computer-controlled pA-meter /DC voltage source (HP-4140B). The device under test was incorporated in a Faraday cage (HP-16055A) to obtain measurements in the dark and/or various illumination levels. A light beam was produced by the Phillips mercury lamp (type CS 50/W3) ,which includes rays in the short-wave ultraviolet part of the spectrum. The beam entered the Faraday cage via an appropriate aperture, thus enabling control of the illumination intensity at three distinct levels. The incoming light power was monitored by a solar sensor ss-100 (Dodge Products) and was set at three different illumination levels, corresponding to the light intensities L_1=0.1mW/cm^2, L_2 = 0.3mW/cm^2 and L_3 = 0.7mW/cm^2.

Typically measured I-V data for the employed devices under the sustained electrical and optical excitation levels are shown in the semi-log diagrams of Fig. 3. Here, due to the logarithmic current presentation, the polarity of the net current flow (i.e., negative values) cannot be exposed. However, the employed log-current scales offer certain advantages in revealing the exponential current dependencies and/or allowing comparisons between currents flowing under forward and reverse bias settings. The effect of increasing the illumination level may be clearly identified in Fig. 3. As predicted by Eqn. (3) for the reverse biased p-n junction, the current will be increased during illumination by the induced photocurrent component.

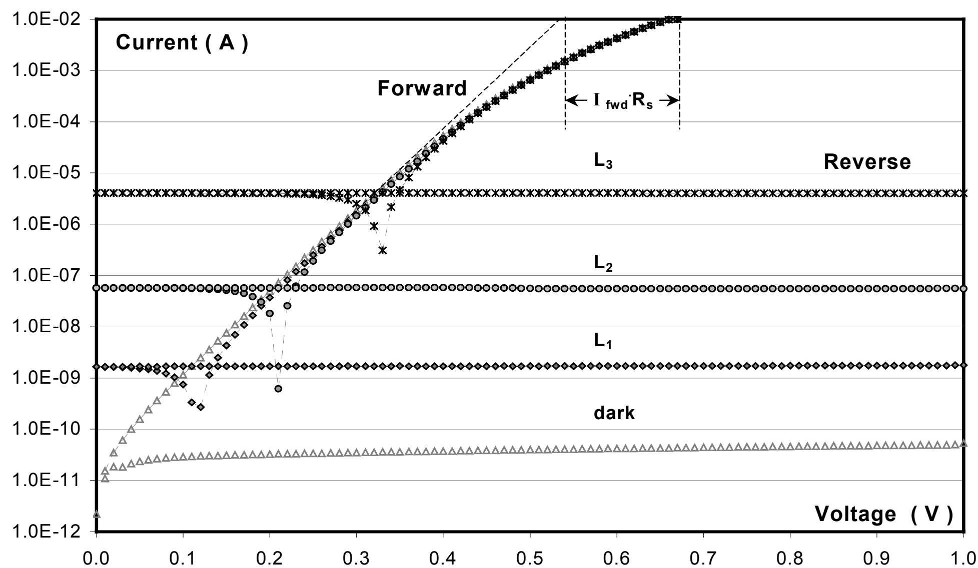

Figure 3. Experimentally obtained I-V curves of an illuminated p-n junction at various incident light power levels, compared to the corresponding response of the same device in the dark. Notice that the reverse bias current increase as the illumination level increases, i.e. dark, L_1 = 0.1 mW/cm^2, L_2 = 0.3 mW/cm^2, L_3 = 0.7 mW/cm^2. The forward bias current drops towards zero values ($I \rightarrow 0$) as the applied forward voltage changes from $V_{fwd} \rightarrow V_{oc}$.

Under forward bias (Eqn. 2), the photocurrent component affects the overall current-voltage characteristics only in the voltage range between $0 < V_{fwd} \leq V_{oc}$, where the photocurrent component is greater by orders of magnitude compared to the current component attributed to the applied forward

polarity. At $V_{fwd} = V_{oc,}$ the two component equity situation is reached, i.e. $I_{fwd} = 0$. Thus, the device open-circuit voltage at each illumination level can be identified by the corresponding forward voltage values, where the total current reduces - by orders of magnitude - towards zero values. Note that as predicted by Eqn. (3), for forward polarities in the range of $0 < V_{fwd} \leq V_{oc}$, the net current has a negative sign, therefore the device produces power. At higher applied forward voltages, the exponential current component dominates and the I-V characteristics appear as straight lines. In this voltage regime, the slope of the logI-V curve allows for the ideality factor (η) the evaluation [5].
Generally, η is a positive number greater than unity, and has to be smaller than 1.06 to ensure for the validity of the quasi-equilibrium model approximation. In other cases, an additional (competitive) charge transport mechanisms may also take place across the potential barrier of the junction. For forward current values greater than approximately 2.10^{-4} A, the observed saturation effect for the examined devices is mainly attributed to the device embedded series resistance, R_s, and/or initiation of the high injection effects [5].

The parametric component values can be evaluated via the measured forward I-V characteristics in the dark, to provide data for the saturation current (I_s), the ideality factor (η) and the series resistance (R_s) of the device under test. According to the experimentally obtained results given in Figure 3 (I-V characteristics in the dark), the reverse bias saturation current is estimated as $I_s = 2.2 * 10^{-11}$ A. In the voltage range, where a linear relationship between ln(I) and V_{fwd} is encountered, the slope of the curve allows for the ideality factor an evaluation; for the specific device it is found to be $\eta = 1.04$. Assuming a bias-independent (linear) series resistance (R_s), the series resistance can be quoted from the measured forward I-V data in the high current region, by the voltage differences (ΔV), obtained between experimentally attained values and the extrapolated line following the exponential I-V relation. As shown in Figure 3, the series resistance will be given by:

$$R_s = \left(V_{fwd}(meas) - V_{fwd}(ideal)\right) / I_{fwd} = \Delta V / I_{fwd} \qquad (8)$$

R_s may be attributed to the bulk resistance of the n- and p-type materials, the metal-semiconductor ohmic contact resistance and the bonding-wire resistance. The obtained experimental values of the exploited physical quantities are summarized in Table 1.

The experimentally produced photocurrent can be evaluated under every applied bias (V_{bias}) and illumination level (L_i) by subtracting the corresponding current values $|I(V_{bias})_{dark} - I(V_{bias})_{Li}|$. According to the above, the bias dependence of the optically generated current, $I_{opt(experimental)}$, can be determined by analyzing the I-V characteristics according to the following equation :

$$I_{opt(exp)}\Big|_{V_{bias}} = I_{TOTAL}(L_i)\Big|_{V_{bias}} - I_{TOTAL}(dark)\Big|_{V_{bias}} \qquad (9)$$

Eqn. (9) allows for the experimental investigation of possible dependencies among major physical quantities determining photo current values, i.e. $I_{opt} = qA(L_n + L_p).g_{opt}$, and the externally applied bias. The applied voltage V_{fwd} or V_{rev} might affect either the minority-carrier diffusion lengths L_n, L_p,

and/or the generation rates g_{opt} of the optically-induced electron hole-pairs. Photocurrent values, quoted under the typical illumination level L_3, are given in Fig. 4. The induced photocurrent is found to be independent of the applied voltages in reverse polarity and independent of the applied forward voltage, providing the applied bias settings are less than V_{oc}. When the applied forward bias exceeds this value, (i.e., $V_{fwd} > V_{oc}$), the produced photocurrent exhibits a strong bias dependence. Notice the exponential photocurrent increase shown in Fig. 4, for applied forward bias settings in the range $V_{fwd} \geq V_{oc}$.

Table 1. Determination of I_s, $I_{opt}(L_i)$, $V_{oc}(L_i)$ and R_s from the experimentally obtained I-V data.

Illumination Level	I_{opt} (A)	V_{oc} (V)	R_s (Ω)
Dark	$I_{opt} = 0$, $I_s = 2.2\text{x}10^{-11}$ A	_	$R_s = (0.67-0.541)\text{V} / 9.97\ \text{x}10^{-3}\ \text{A} \Rightarrow R_s = 12.94\ \Omega$
$L_1 = 0.1$ mW/cm^2	$I_{opt}^* = 1.67\ \text{x}10^{-9}$ A	0.12 V	$100\ \Omega \leq R_s^* \leq 3\ \text{k}\Omega$ (bias-dependent)
$L_2 = 0.3$ mW/cm^2	$I_{opt}^* = 5.52\ \text{x}10^{-8}$ A	0.21 V	
$L_3 = 0.7$ mW/cm^2	$I_{opt}^* = 4.02\ \text{x}10^{-6}$ A	0.33 V	

*Quoted value for reverse biased junction, or forward-biased having $V_{app} < V_{oc}$

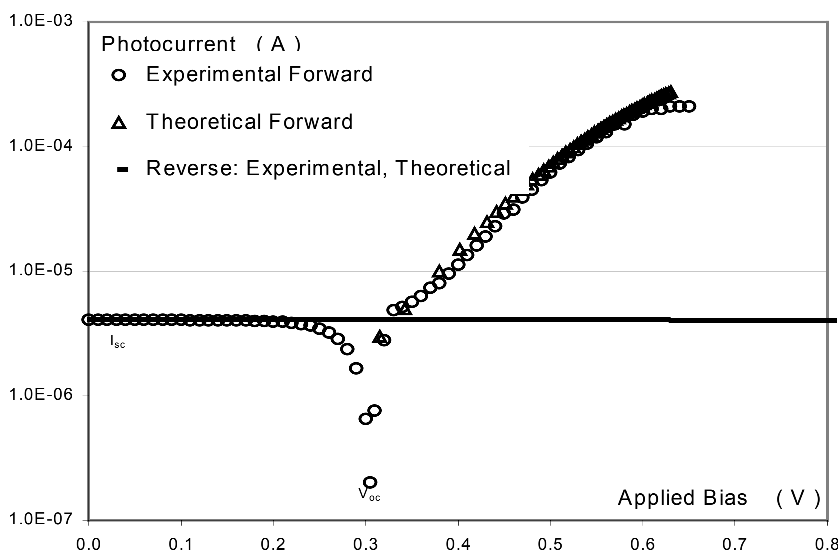

Figure 4. The experimentally obtained photocurrent under illumination level $L_3 = 0.7$ mW/cm^2 appears to be independent of the applied potential only when $V_{applied} < V_{oc}$. For forward voltages $V_{fwd} > V_{oc}$, the optically generated current $I_{opt(Vfwd)}$ increases exponentially with the applied bias towards a saturation value and may be mathematically described by Eqn. (12). The simulated photocurrent-voltage data for the selected reference values of V_{oc}, I_{opt} and R_s* are also given in the same plot for comparison purposes.

Simulated I-V Curves for an Illuminated p-n Junction

The current-voltage response of p-n junctions sustaining simultaneously optical and electrical excitation may be evaluated by comparing the experimentally attained data to the theoretically predicted response. Theoretical I-V curves can be obtained by applying Eqn. (10) and (11).

$$I_{fwd} = I_s \cdot \left(e^{\frac{q\left(V_{fwd} - I_{fwd} R_s\right)}{\eta kT}} - 1 \right) - I_{opt} \tag{10}$$

$$I_{rev} = I_s + I_{opt} \tag{11}$$

Measurements of the current-voltage characteristics in the dark have been utilized to provide reference values for the reverse bias saturation current I_s, the ideality factor η and the series resistance R_s, of the device under test. Similar measurements under different illumination levels L_i provide the reference values for the generated photocurrent as well as for the corresponding open circuit voltage. By substituting these values into Eqn. (10) and (11), one can get the simulated I-V curves of the examined p-n junction under forward and reverse polarity at the applied illumination levels. These I-V plots are presented in Fig. 5 and they were obtained by substituting for I_{opt}, I_s, R_s and η, the data of Table 1 and by applying Eqn. (10) and (11). The simulated curves are closely compared to the experimentally obtained I-V data, as shown in Fig. 6 and Fig. 7.

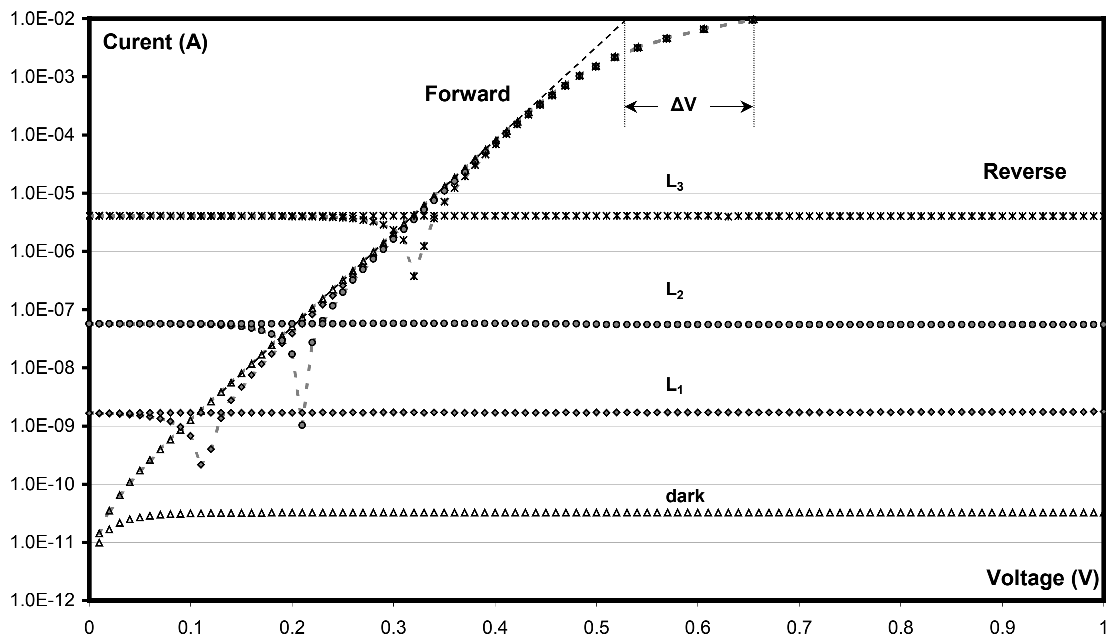

Figure 5. Theoretically evaluated I-V curves at various illumination levels (i.e., dark, L_1, L_2, L_3) for a p-n junction having the following parametric data: $I_s = 2.2 \times 10^{-12}$ A, η=1.04, R_s = 12.94 Ω. The substituted reverse bias photocurrent values were: $I_{opt}(L_1) = 1.67 \times 10^{-9}$ A, $I_{opt}(L_2) = 5.52 \times 10^{-8}$ A, and $I_{opt}(L_3) = 4.02 \times 10^{-6}$ A. Notice remarkable similarities to the experimentally obtained curves of Fig. (2).

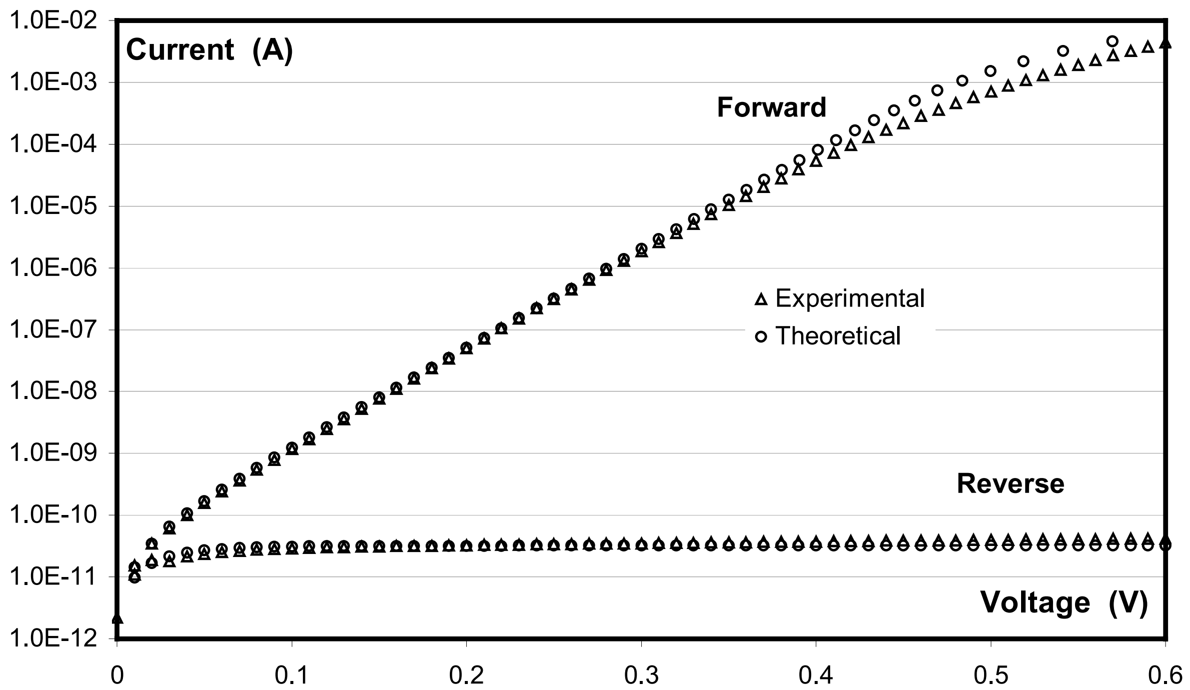

Figure 6. Close comparison between the experimental I-V curves and the theoretical ones in the dark. Only minor discrepancies appear under forward polarity at moderate applied voltages.

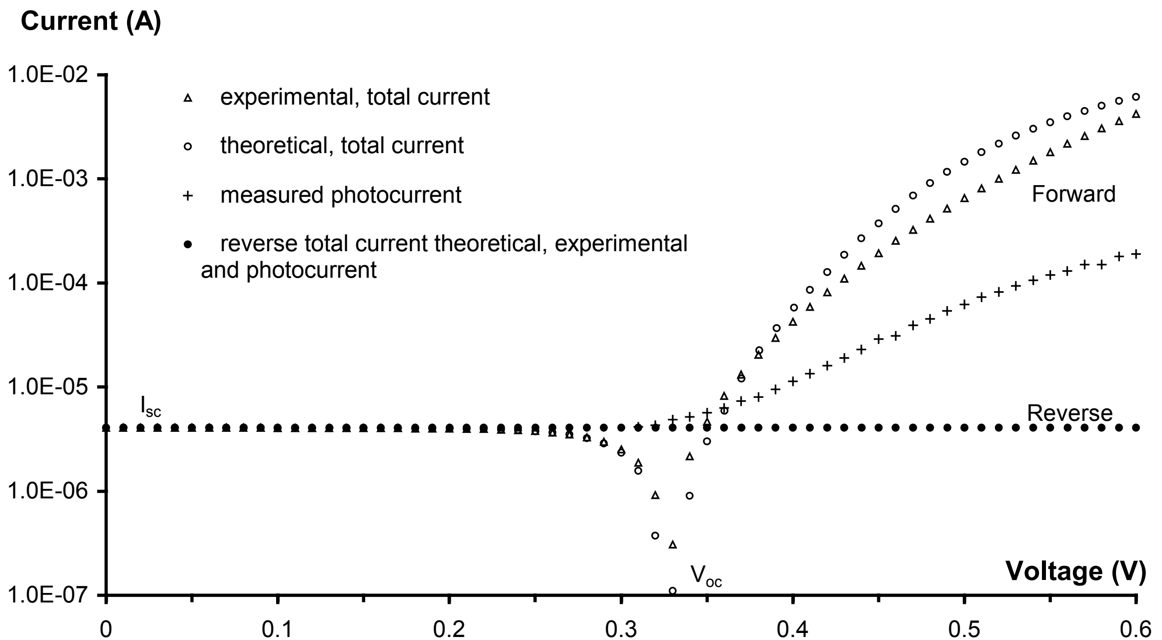

Figure 7. The experimentally and theoretically obtained I–V characteristics of the device under the illumination level L_3. The measured photocurrent is also incorporated in the same plot for comparison purposes.

So far, the evaluation of the I-V curves has been based upon the existing theory of an ideal p-n junction, i.e. the effect of recombination centres, the operating temperature, and high injection processes have not been considered. In addition, the produced photocurrents are assumed to be independent of the applied bias. However, as shown by the experimental results of Fig. 4, the produced photocurrent is bias-dependent for applied forward voltages $V_{fwd} > V_{oc}$. In this voltage region, the optically produced current may be given by an equation of the following form:

$$I_{opt(V_{fwd})} = I_{opt} \cdot \left(e^{\left(\frac{q \cdot \left(V_{fwd} - V_{oc} - I_{opt(V_{fwd})} \cdot R_s^* \right)}{2 \cdot k \cdot T} \right)} \right) \qquad \text{for } V_{fwd} > V_{oc}$$

$$I_{opt(V_{fwd})} \to 0 \qquad \text{for } V_{fwd} \to V_{oc} \qquad (12)$$

$$I_{opt(V_{fwd})} = I_{opt(rev)} = I_{opt} = constant \qquad \text{for } V_{appl(fwd,\ rev)} < V_{oc}$$

where I_{opt} is the optically induced current in reverse bias. The slope of the photocurrent $\log(I_{opt})$-V_{fwd} curve is 2.k.T/q, as predicted by Eqn. (5) for recombination currents under forward bias. The evaluated photocurrent data according to Eqn. (12) have been superimposed on the experimental data of Fig. 4 for comparison purposes. The simulated curves were quoted by employing the following values for the physical quantities of Table 1: Reverse bias photocurrent corresponding to illumination level L_3, $I_{opt} = 4.02 \times 10^{-6}$ A, open circuit voltage under the same illumination $V_{oc} = 0.33$ V, and photocurrent saturation series resistance $R_s^* = 300\ \Omega$. According to the obtained experimental results, the saturation series resistance appears as a non-linear physical quantity depending on the current and applied voltage values. It was confirmed that for the employed devices, R_s^* tends to increase drastically with the applied bias towards 3 kΩ values in the high photocurrent region (see Fig. 4).

This photocurrent saturation effect could be attributed to the unelastic carrier transport processes developing as the junction temperature increases. The factor $q.V_{fwd}/2.k.T$ at the exponential of Eqn. (12) also appears in Eqn. (5) giving the recombination current density. It may thus, be assumed that for $V_{fwd} \gg V_{oc}$ the photocurrent is mainly a recombination current, so that:

$$I_{opt(V_{fwd})} = I_{rec} = A \cdot J_{rec} \qquad (13)$$

where A is the area of the device. By substituting to the above equation for $I_{opt(Vfwd)}$ and J_{rec} from Eqn. (12 and 5), respectively, it can be found that:

$$I_{opt(V_{fwd})} \cdot R_s^* = \frac{2 \cdot k \cdot T}{q} \ln\left(\frac{2 \cdot \tau_o \cdot I_{opt}}{A \cdot q \cdot w \cdot n_i} \right) - V_{oc} \qquad (14)$$

The open circuit voltage V_{oc}, given in Eqn. (1), may be transformed to [8]:

$$V_{oc} = \frac{k \cdot T}{q} \ln\left(\frac{I_{opt}}{I_s} + 1 \right) \qquad (15)$$

The included term +1 in Eqn. (15) may be practically omitted since $I_{opt} >> I_s$ (according to the obtained experimental results given in Table 1). By substituting for I_s from Eqn. (4) into Eqn. (15) and feeding-in the obtained expression of V_{oc} into Eqn. (14), one can come to the conclusion that:

$$R_s^* = \frac{1}{I_{opt}(V_{fwd})} \cdot \frac{k \cdot T}{q} \ln\left[\frac{4 \cdot \tau_o^2 \cdot I_{opt}}{A \cdot q \cdot w^2} \cdot \left(\frac{D_n}{N_A \cdot L_n} + \frac{D_p}{N_D \cdot L_p}\right)\right] \tag{16}$$

According to Eqn. (16), for a given current value the series resistance R_s* is increased with the junction temperature. Other included quantities such as the reverse bias photocurrent I_{opt} or the diffusion lengths L_p, L_n vary in comparison rather weakly with the junction temperature. Therefore, R_s* will increase with temperature. This may explain the photocurrent saturation response observed under high forward voltage and current values, where the junction temperature is significantly increased.

Finally, it should be stated that additional processes introducing deviations from the theoretically predicted response are high injection effects [12] developing under forward bias, whose mechanisms are not yet adequately exploited.

Conclusion

The experimental investigation of the current-voltage response of illuminated p-n junctions in forward and reverse polarity enables for the experimental evaluation of the produced photocurrent as a function of the applied bias and given illumination level. Under reverse bias, i.e. the third quadrant of the I-V characteristics where the p-n junction is normally utilized as a *photodetector*, the produced photocurrent is constant and independent of the applied bias. Under forward applied bias $V_{fwd} \leq V_{oc}$, i.e. the fourth quadrant of the I-V characteristics where, the p-n junction is normally utilized as a *photovoltaic cell*, the produced photocurrent remains bias-independent but rapidly tends towards zero values as $V_{fwd} \rightarrow V_{oc}$. For applied forward biases beyond the open circuit voltage, i.e. the first quadrant of the I-V characteristics, where the p-n junction is normally operated, the produced photocurrent increases exponentially with the applied bias attaining a 2kT/q slope in the semi-log (I-V) plot due to recombination effects. For the optically induced current component the corresponding series resistance appears to be bias dependent and has to be modelled as a non-linear physical quantity (though the series resistance of the same device in the dark is linear and independent of the applied voltage or developing current values).

By feeding some p-n junction reference values obtained experimentally from the I-V characteristics in the dark to Eqn.(10, 11, and 12), the generalized current-voltage characteristics can be predicted very closely at any illumination level. Discrepancies between the experimental and theoretical I-V curves help towards validating the existing quasi equilibrium models. The recombination theory, the temperature dependence of the p-n junction characteristics and the high injection effects could be some of the causes initiating such discrepancies. Thus, the above described approach enables the theoretical and experimental investigation of the optically induced current components, and helps towards the modelling of the physical quantities of semiconducting materials (i.e., I_{opt}, R_s*, L_n, L_p).

References

1. Keller, S.; Spiegel, M.; Fath, P.; Willeke, G.P.; Bucher, E. Critical evaluation of the effective diffusion length determination in crystalline silicon solar cells from an extended spectral analysis, *IEEE Transactions on Electron Devices,* **1998**, 45(7), 1569.

2. Adjakou, R.; Lishou, C.; Dieye, N.; Protin, L. Using state-space representation for the modelisation of photovoltaic systems, *Applied Mathematics and Computation*, **2001**, 124, 129.

3. Ikegami, T.; Maezono, T.; Nakanishi, F.; Yamagata, Y.; Ebihara, K. Estimation of equivalent circuit parameters of PV module and its application to optimal operation of PV system, *Solar Energy Materials & Solar Cells*, **2001**, 67, 389.

4. Gautam, N. K.; Kaushika, N.D. An efficient algorithm to simulate the electrical performance of solar photovoltaic arrays, *Energy*, **2002**, 27, 347.

5. Carroll, J.E. Physical Models for Semiconductor Devices, Edward Arnold, Cambridge, **1980**.

6. Sah, C.T.; Noyce, R.N.; Shockley, W. in: Proc. IRE '57, Carrier generation and recombination in p-n junctions and p-n junction characteristics, **1957**, 45, 1228.

7. Streetman, B.G. Solid State Electronic Devices, Prentice Hall, New Jersey, **1980**.

8. Navon, D.H. Semiconductor Microdevices and Materials, CBS College Publishing, New York, **1986**.

9. Moll, J.L. Physics of Semiconductor Devices, McGraw Hill Book Co., New York, **1964**.

10. Shockley, W.; Read, W.T. Statistics of the recombination of holes and electrons, *Phys. Rev*., **1952**, 87, 853.

11. Grove, A.S. Physics and Technology of Semiconductor Devices, John Wiley & Sons Inc, New York, **1967**.

12. Sze, S.M. Physics of Semiconductor Devices, 2nd Ed. Wiley, New York, **1981**.

© 2004 by MDPI (http://www.mdpi.org). Reproduction is permitted for noncommercial purposes.